the FEBS Journal

A single intersubunit salt bridge affects oligomerization and catalytic activity in a bacterial quinone reductase

Alexandra Binter[1], Nicole Staunig[2], Ilian Jelesarov[3], Karl Lohner[4], Bruce A. Palfey[5], Sigrid Deller[1], Karl Gruber[2] and Peter Macheroux[1]

1 Institute of Biochemistry, Graz University of Technology, Austria
2 Institute of Molecular Biosciences, University of Graz, Austria
3 Institute of Biochemistry, University of Zürich, Switzerland
4 Institute of Biophysics and Nanosystems Research, Austrian Academy of Sciences, Graz, Austria
5 Department of Biological Chemistry, University of Michigan, Ann Arbor, MI, USA

Keywords
NADPH:FMN oxidoreductase; oligomerization; quinone reductase; salt bridge; thermostability

Correspondence
K. Gruber, Institute of Molecular Biosciences, University of Graz, Humboldtstrasse 50/III, A-8010 Graz, Austria
Fax: +43 316 380 9897
Tel: +43 316 380 5483
E-mail: karl.gruber@uni-graz.at
P. Macheroux, Institute of Biochemistry, Graz University of Technology, Petersgasse 12/II, A-8010 Graz, Austria
Fax: +43 316 873 6952
Tel: +43 316 873 6450
E-mail: peter.macheroux@tugraz.at

(Received 25 May 2009, revised 14 July 2009, accepted 17 July 2009)

doi:10.1111/j.1742-4658.2009.07222.x

YhdA, a thermostable NADPH:FMN oxidoreductase from *Bacillus subtilis*, reduces quinones via a ping-pong bi-bi mechanism with a pronounced preference for NADPH. The enzyme occurs as a stable tetramer in solution. The two extended dimer surfaces are packed against each other by a 90° rotation of one dimer with respect to the other. This assembly is stabilized by the formation of four salt bridges between K109 and D137 of the neighbouring protomers. To investigate the importance of the ion pair contacts, the K109L and D137L single replacement variants, as well as the K109L/D137L and K109D/D137K double replacement variants, were generated, expressed, purified, crystallized and biochemically characterized. The K109L and D137L variants form dimers instead of tetramers, whereas the K109L/D137L and K109D/D137K variants appear to exist in a dimer–tetramer equilibrium in solution. The crystal structures of the K109L and D137L variants confirm the dimeric state, with the K109L/D137L and K109D/D137K variants adopting a tetrameric assembly. Interestingly, all protein variants show a drastically reduced quinone reductase activity in steady-state kinetics. Detailed analysis of the two half reactions revealed that the oxidative half reaction is not affected, whereas reduction of the bound FMN cofactor by NADPH is virtually abolished. Inspection of the crystal structures indicates that the side chain of K109 plays a dual role by forming a salt bridge to D137, as well as stabilizing a glycine-rich loop in the vicinity of the FMN cofactor. In all protein variants, this glycine-rich loop exhibits a much higher mobility, compared to the wild-type. This appears to be incompatible with NADPH binding and thus leads to abrogation of flavin reduction.

Structured digital abstract

- MINT-7229866, MINT-7229874, MINT-7229885, MINT-7229894, MINT-7229905: *YhdA* (uniprotkb:O07529) and *YhdA* (uniprotkb:O07529) *bind* (MI:0407) by *blue native page* (MI:0276)
- MINT-7229854: *YhdA* (uniprotkb:O07529) and *YhdA* (uniprotkb:O07529) *bind* (MI:0407) by *x-ray crystallography* (MI:0114)

Abbreviations
DSC, differential scanning calorimetry; DLS, dynamic light scattering; Ni-NTA, nickel-nitrilotriacetic acid agarose.

Introduction

The search for enzymes with catalytic properties of potential application in biocatalysis and biotechnology has led to the discovery of bacterial enzymes known as azoreductases. These enzymes are found in several diverse bacterial species catalysing the reductive cleavage of azo dyes containing one or more azo-bonds (R_1-N=N-R_2) to their corresponding amines [1–7]. Aromatic azo dyes are artificial chemicals with potentially harmful properties resulting in health and environmental concerns. Recently, we described a FMN-containing flavoenzyme from *Bacillus subtilis*, termed YhdA, capable of cleaving azo dyes such as Cibachron Marine (Ciba, Basel, Switzerland) at the expense of NADPH [8]. YhdA shares sequence similarity with a family of flavin- (FMN or FAD) dependent quinone reductases such as mammalian NQO1 and yeast Lot6p [9]. Moreover, YhdA and these eukaryotic quinone reductases possess a similar protein topology, a so-called flavodoxin fold consisting of five α-helices sandwiching a five-stranded parallel β-sheet in the centre [10,11]. Because of these similarities, we were interested in analyzing whether YhdA accepts quinones as substrates. In the present study, it is demonstrated that the enzyme reduces a variety of quinones by a ping-pong bi-bi kinetic mechanism with a clear preference for NADPH as reducing agent. As could be expected, the turnover rates for quinones are much higher than those obtained for artificial azo-compounds, in line with the assumption that quinones, unlike azo dyes, are cognate enzyme substrates.

Bacterial and eukaryotic quinone reductases possess a similar protein topology, but diverge with respect to their oligomeric structure. Although eukaryotic proteins form dimers, YhdA and Azo1 (from *Staphylococcus aureus*) [4] form tetramers [8,9]. In the case of YhdA, the tetramer is formed by two dimers, which interact through an extended concave surface. The interface between dimers is stabilized by four salt bridges formed by the side chains of residues K109 and D137 of structural neighbours (Scheme 1). This higher oligomerization state was considered to be responsible for the increased thermal stability of YhdA (T_m = 87 °C) compared to the dimeric yeast homolog Lot6p (T_m = 60.2 °C) [12]. To test this hypothesis and to obtain more insight into the importance of these salt bridges for tetramer assembly, we created four YhdA protein variants: K109L, D137L, K109L/D137L and K109D/D137K. Characterization of the variants showed that single replacement of K109 or D137 disrupts the tetramer, whereas the two double replacement protein variants appear to have conserved some tendency to form tetramers. Interestingly, all of the

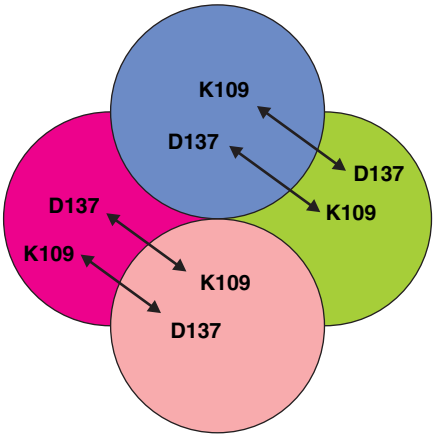

Scheme 1. Schematic representation of the four salt-bridges in the YhdA tetramer. One dimer is formed by the green and magenta chains; the second by the pink and blue chains.

variants have a melting point similar to the wild-type protein, suggesting that the high thermostability is an intrinsic property of the dimer. Surprisingly, the protein variants showed dramatically reduced enzymatic activity, which is a result of the breakdown of the reductive half reaction, indicating that structural changes impede docking of NADPH to the active site. Crystallization and concomitant X-ray crystallographic determination of variant structures revealed that increased mobility of a highly conserved glycine-rich loop in the vicinity of the isoalloxazine ring system might be responsible for the loss of enzyme activity.

Results

YhdA has recently been classified as an NADPH:FMN oxidoreductase with the ability to reductively cleave azo dyes [8]. Lot6p, the YhdA homolog in yeast, was shown to reduce quinones to their hydroquinone state [12]; hence, we tested YhdA for its quinone reductase activity. Steady-state measurements using several quinone substrates as electron acceptors resulted in much higher turnover rates than those reported for the reduction of azo dyes (data not shown). For a more detailed characterization, 2-hydroxy-*p*-naphthoquinone was chosen as a representative substrate. Figure 1 shows the double reciprocal plot of initial velocity measurements in the presence of NADPH as the electron donor and 2-hydroxy-*p*-naphthoquinone as electron acceptor. The family of parallel lines obtained from data analysis indicates a ping-pong bi-bi mechanism, where both substrates consecutively bind to the catalytic site (i.e. the electron donor NADPH binds first, then dissociates

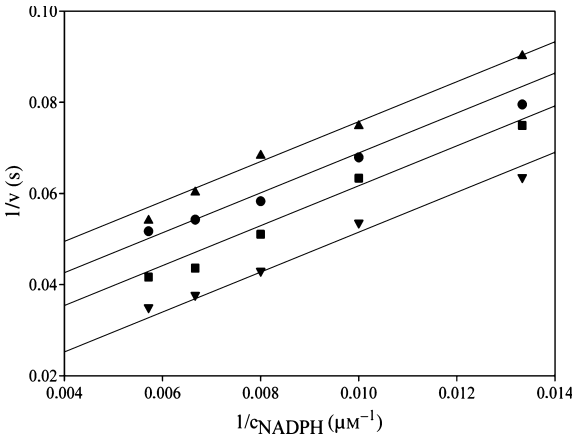

Fig. 1. Double-reciprocal plot of initial rate measurements in steady-state experiments as a function of NADPH at 2 (▲), 5 (●), 10 (■) and 30 (▼) μM of 2-hydroxy-*p*-naphthoquinone (from top to bottom).

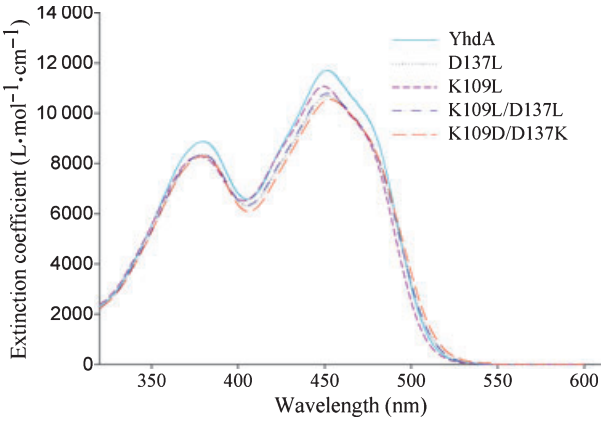

Fig. 2. UV/visible absorbance spectra of wild-type YhdA and the four protein variants.

to vacate the active site for binding of the electron accepting quinone substrate). The same mechanism was proposed for the homologous yeast enzyme Lot6p and other quinone reductases [12].

Using [*S*-^{2}H]-NADPH and [*R*-^{2}H]-NADPH as reducing agents and subsequent analysis of $NADP^+$ by ^{1}H-NMR spectroscopy, it was revealed that the pro-*S* hydride of NADPH is preferentially transferred to FMN.

Heterologous expression of the four generated protein variants was performed in the same way as that described for wild-type protein, resulting in similar amounts of soluble protein. All hexahistidine-tagged protein variants were purified by nickel-nitrilotriacetic acid agarose (Ni-NTA) chromatography according to the protocol established for wild-type YhdA. YhdA possesses a noncovalently bound FMN cofactor, which is also present in the protein variants, but showed some minor changes in their UV/visible absorbance spectra (Fig. 2). The extinction coefficients of enzyme-bound FMN were determined using an extinction coefficient of ε_{450} = 12 400 $M^{-1}\cdot cm^{-1}$ for free FMN and are summarized in Table 1.

The native molecular mass was estimated by molecular sieve chromatography. Each protein variant eluted as a single species; however, all protein variants exhibited larger elution volumes indicating a lower apparent mass (Table 2). These data suggest that the two single protein variants and the K109L/D137L double protein variant form dimers in solution. On the other hand, the K109D/D137K variant showed a native molecular mass of 61 kDa, suggesting that the protein may exist in a dimer–tetramer equilibrium. This result was qualitatively confirmed by dynamic light scattering (DLS) experiments (Table 2), demonstrating that the single replacement variants form dimers rather than tetramers. On the other hand, both double replacement protein variants show a tendency to form a tetramer similar to wild-type protein.

Table 1. Extinction coefficients of wild-type YhdA and the four protein variants at 450 nm.

Protein	ε_{450} ($M^{-1}\cdot cm^{-1}$)	λ_{max} (nm)
Wild-type	11 690	451
D137L	10 660	452
K109L	11 070	450
K109L/D137L	10 760	452
K109D/D137K	10 720	453

Table 2. Native molecular mass estimation by molecular sieve chromatography and DLS and apparent unfolding temperatures T_m in °C as determined by CD spectroscopy and DSC. The void volume of the column was determined to V_o = 44.04 mL.

Protein	V_E (mL)	Molecular mass (kDa)	DLS[a] (kDa)	T_m (CD)	T_m (DSC)
Wild-type	56.69	72.7	85	87[b]	93
D137L	66.29	33.5	53	84	95
K109L	64.61	44.0	68	88	95
K109L/D137L	64.21	45.1	72	89	95
K109D/D137K	59.45	61.0	88	89	> 95

[a] The values given are the average of two independent measurements. [b] Value taken from [8].

To further characterize the oligomerization of the protein variants, native PAGE was employed. As shown in Fig. 3A, both single protein variants have a higher mobility compared to wild-type protein; this can be interpreted in terms of the formation of dimers

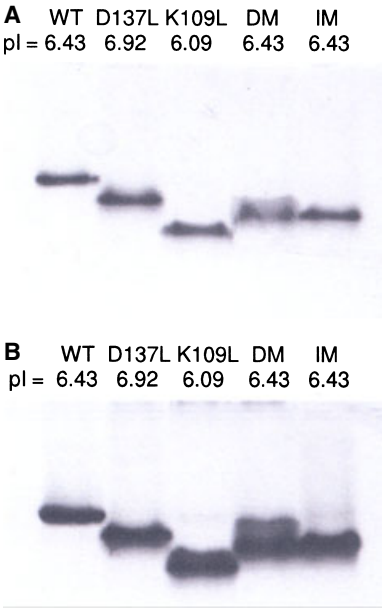

Fig. 3. Native PAGE. From left to right, WT = YhdA wild-type, D137L variant, K109L variant; DM = K109L/D137L variant, IM K109D/D137K variant. Protein solution (6.5 μL) at (A) 15 μM and (B) 60 μM, respectively, was applied onto each lane.

rather than tetramers. The different isoelectric points resulting from the aspartate to leucine (pI = 6.92) and the lysine to leucine (pI = 6.09) replacements, respectively, account for the mobility shift between the two single protein variants. The two double protein variants give rise to bands positioned between the K109L and D137L variant. Considering that the two double protein variants have an intermediate isoelectric point of 6.43 (i.e. the same as wild-type protein), this result also suggests that both of these protein variants occur as dimers. However, at higher protein concentrations (Fig. 3B; and barely visible in Fig. 3A), the K109L/D137L protein variant exhibits an additional band at lower mobility, indicating that this protein variant may form tetramers under these conditions. Interestingly, the 'inverse' K109D/D137K variant produces only a single band at high mobility (no change between Fig. 3A, B) in contrast to the dimer–tetramer equilibrium suggested by molecular sieve chromatography. Obviously, both double replacement variants have some tendency to form tetramers, albeit much weaker than the wild-type protein.

Next, we characterized the protein variants with respect to their quinone reductase activity. Initial rate measurements show that all protein variants retain less than 1% of wild-type activity, using molecular oxygen as well as various quinones as final electron acceptors (Table 3). Stopped-flow measurements were performed to determine whether the reductive or the oxidative half reaction is impaired in the protein variants. The reductive half reaction of wild-type, the D137L and the K109L/D137L protein variant was investigated in more detail. With both protein variants, the rate of reduction of the FMN cofactor was very small, amounting to 0.6% and 3% of the wild-type rate for the D137L and K109L/D137L protein variants, respectively. The rate of reduction for the other two protein variants was much smaller and could not be determined accurately in the stopped-flow instrument. On the other hand, the oxidative half reaction using 2-hydroxy-*p*-naphthoquinone as a substrate was not affected in any of the protein variants, yielding comparable rates for wild-type and all protein variants (Table 3). Hence, it can be concluded that the loss of enzymatic activity in the four protein variants observed in steady-state measurements is a result of the collapse of the reduction step (i.e. the transfer of electrons from NADPH to the flavin cofactor).

YhdA has been described as an enzyme exhibiting high thermostability with a melting temperature of 86.5 °C, as determined by monitoring thermal unfold-

Table 3. Steady-state and rapid reaction parameters for wild-type YhdA and protein variants. Turnover measurements were carried out with NADPH and oxygen as substrates. The rate of reduction and oxidation was measured with NADPH and 2-hydroxy-*p*-naphthoquinone (2OH*p*NQ), respectively. ND, not determined (rates were very small compared to wild-type YhdA).

Protein	Turnover (s^{-1})	K_M (NADPH) (mM)	Reduction k_{red} (s^{-1})	K_D (NADPH) (mM)	Oxidation k_{ox} (s^{-1})	K_D (2OH*p*NQ) (mM)
Wild-type	57.9 ± 6.7	0.52 ± 0.09	100 ± 3	0.54 ± 0.05	90 ± 9.7	0.27 ± 0.05
D137L	0.28 ± 0.02	0.65 ± 0.07[a]	0.45[b]	–	115 ± 7.1	0.21 ± 0.02
K109L	0.02 ± 0.004	0.42 ± 0.14[a]	ND	–	96 ± 28.8	0.31 ± 0.018
K109L/D137L	0.55 ± 0.12	1.37 ± 0.35[a]	3.07 ± 0.3	2.29 ± 0.42	103 ± 10.9	0.24 ± 0.044
K109D/D137K	0.16 ± 0.04	0.69 ± 0.18[a]	ND	–	124 ± 6.6	0.12 ± 0.014

[a] Accurate determination of K_M values was hampered by low activity of the variants. [b] Rate of reduction increased linearly to k_{red} = 0.45 s^{-1} at 4 mM NADPH.

ing of the protein by CD spectroscopy [8]. The high thermostability of the tetrameric YhdA in comparison to its dimeric yeast homologue Lot6p (T_m = 60 °C) gave rise to the assumption that the tetrameric state stabilizes the protein toward thermal unfolding [13]. Both proteins possess a common structural topology, the so-called flavodoxin-like fold. They exhibit the same dimer architecture, forming a large, slightly concave surface, characterized by four α-helices spanning its entire width [11]. In the case of Lot6p, several charged residues in the central part of this surface appear to interfere with the tetrameric assembly. These residues are replaced by hydrophobic or uncharged residues in YhdA, which allows tetramer formation by rotating the two dimers against each other by 90° and packing of the two dimers. To test the hypothesis that tetramerization is responsible for increased thermostability, the apparent melting temperatures of the protein variants were determined by CD spectrometry and differential scanning calorimetry (DSC). Surprisingly, no significant changes in the thermostability of the protein variants were observed (Table 2). Thus, it can be concluded that the higher oligomerization state of YhdA compared to Lot6p is not the governing factor for achieving higher thermostability because all four predominantly dimeric protein variants show unfolding temperatures similar to the tetrameric wild-type protein.

All four YhdA variants were crystallized. Three structures (of the K109L, the D137L and K109D/D137K variant) were determined and refined to varying crystallographic resolution (Table 4). The crystals obtained for the K109L/D137L variant were isomorphous to the hexagonal crystal form of wild-type YhdA [Protein Data Bank (PDB) entry: 1NNI] but diffracted to lower resolution; therefore, this structure was not refined further.

The YhdA protomer belongs to the SCOP family [14] of 'NADPH-dependent FMN reductases'. The closest structural neighbours, according to a SSM analysis [15], are a NAD(P)H-dependent FMN reductase from *Pseudomonas aeruginosa* (PDB entry: 1x77) [16], ArsH from *Sinorhizobium meliloti* (2q62) [17], a NADH-dependent FMN reductase from the EDTA-degrading bacterium bnc1 (2vzf, 2vzh, 2vzj) [18] and ArsH from *Shigella flexneri* (2fzv) [19]. The rmsd are in the range 1.6–2.0 Å for 150–160 aligned C-α atoms.

The oligomeric states of the different variants in the crystalline state were analyzed using the MSD-PISA server [20] taking into account all the interactions of protein chains within the asymmetric unit as well as with symmetry equivalent molecules. The crystal

Table 4. Data collection and refinement statistics. Values in parentheses are for highest-resolution shell.

	K109L	D137L	K109D/D137K
Data collection			
Space group	$P22_12_1$	$P1$	$P2_1$
Cell dimensions			
a, *b*, *c* (Å)	47.54, 66.24, 220.75	51.49, 56.08, 64.18	68.63, 170.13, 93.29
α, β, γ (°)	90.0, 90.0, 90.0	84.1, 77.0, 74.5	90.0, 92.3, 90.0
Resolution (Å)	29.0–3.20 (3.31–3.20)	20.0–2.40 (2.44–2.40)	30.0–2.11 (2.16–2.11)
R_{sym}	0.161 (0.597)	0.057 (0.274)	0.096 (0.460)
$I/\sigma I$	10.4 (2.9)	12.8 (3.2)	15.8 (2.0)
Completeness (%)	99.5 (99.5)	95.0 (88.8)	96.7 (52.5)
Redundancy	4.9 (4.5)	2.0 (1.9)	3.6 (2.0)
Refinement			
Resolution (Å)	29.0–3.20	19.9–2.50	29.3–2.11
Number of reflections	12 155	24 878	119 393
R_{work}/R_{free}	0.212/0.262	0.199/0.251	0.185/0.221
Number of atoms			
Protein	5124	5175	15 379
Cofactor	124	124	372
Water	–	319	977
B-factors			
Protein	58.0	36.5	36.1
Cofactor	53.6	28.3	29.4
Water	–	39.3	40.7
rmsd			
Bond lengths (Å)	0.003	0.002	0.002
Bond angles (°)	0.6	0.6	0.6

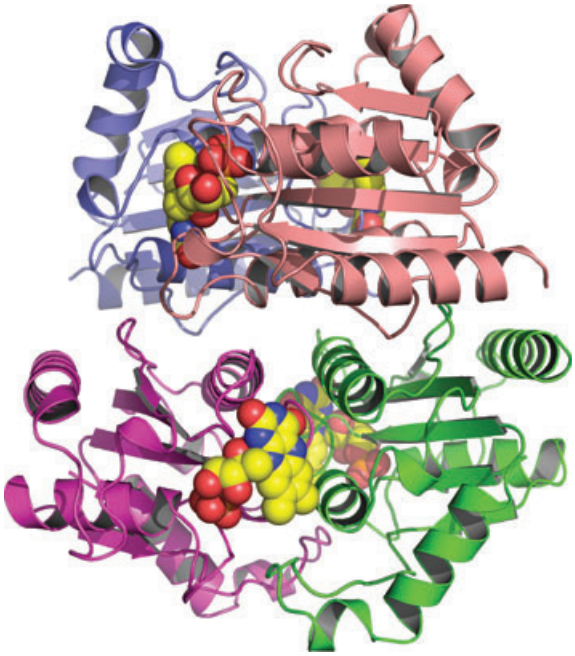

Fig. 4. Crystal structure of wild-type YhdA from *Bacillus subtilis* (PDB entry: 1NNI). The oligomeric state can be described as a dimer of dimers. One dimer is formed by the green and magenta chains; the second by the pink and blue chains. The FMN cofactors are shown as spheres. The figure was prepared using the software PYMOL (http://www.pymol.org/).

structure of wild-type YhdA contains only one protein chain in the asymmetric unit, but a tetramer is formed by two crystallographic diads (space group $P6_222$), which is predicted to be stable also in solution. This prediction was confirmed experimentally by molecular sieve chromatography and native PAGE (Fig. 3 and Table 2). This tetramer exhibits 222 symmetry and can be considered as a dimer of dimers (Fig. 4) with a significantly larger interaction surface within the dimers (~ 1100 Å^2 buried surface area per chain) than between them (~ 660 Å^2). Four individual salt bridges involving K109 and D137 are formed across the dimer–dimer interface (Scheme 1). Lys109 also forms hydrogen bonds to three carbonyl groups in the glycine rich loop (G^{106}-GG-K^{109}-GG^{111}) of the neighbouring subunit, thereby stabilizing this loop, which is in close proximity of the N(1)-C(2 = O) locus of the flavin (Fig. 5). Based on the observed isomorphicity of crystals obtained for the K109L/D137L variant, the same oligomeric state can safely be assumed to be present, although the salt bridge between Lys109 and Asp137 cannot be formed in this case. Most of the closest structural neighbours mentioned above also form tetramers in the crystal, and the mode of oligomerization is the same as in YhdA. The only exception is the NAD(P)H-dependent FMN reductase from *P. aeruginosa*, which forms a dimer again equivalent to YhdA. In this context, it is noteworthy that K109 and D137 are only conserved among putative oxidoreductases in the genera *Bacillus* and are not found in any of the other structurally related proteins. This clearly indicates that tetramer formation is not solely dependent on the presence of the salt bridges formed between these residues.

The asymmetric unit of crystals of the K109D/D137K variant contains 12 protein chains forming three tetramers, which are each very similar to the wild-type tetramer. rmsd were in the range 0.3–0.4 Å after superposition of 664–669 C-α atoms (> 90% of the total number of C-α atoms in the tetramers). Although, in principle, the 'inverse' amino acid exchange should allow the formation of an inter-dimer salt bridge, this interaction is not observed in the crystal structure. In addition, the stabilizing interactions of the lysine with the carbonyl groups in the glycine rich loop in the neighbouring protomer are not formed (Fig. 5). Accordingly, PISA analysis predicts a lower stability for this tetramer (calculated ΔG_{diss} = 4.5–6.2 kcal·mol^{-1} compared to 9.8 kcal·mol^{-1} for native YhdA) which thus could more easily dissociate into dimers in solution.

The remaining two variants (K109L and D137L) show different oligomeric states in each case, with four protomers in the asymmetric unit, which form two dimers identical to the dimers found in the other YhdA structures. In the crystal, these two dimers also form tetramers, which, according to the PISA analysis, should only be marginally stable in solution (ΔG_{diss} of −0.1 and 1.4 kcal·mol^{-1}). These tetramer arrangements are very similar in the two structures (rmsd of 0.6 Å for 626 superimposed C-α atoms). Compared to the wild-type tetramer, the two dimers interact differently with each other. Although, in wild-type YhdA (as well as in the studied double mutant proteins), the two dimers are aligned almost perpendicular to each other, they are essentially parallel in the single mutant proteins (Fig. 6).

The isolated protomers of the YhdA variant structures show only small structural changes compared to the wild-type (rmsd in the range 0.3–0.6 Å for 166–168 superimposed C-α atoms). The largest changes are observed in the region around residue 109, which is in the centre of the above mentioned glycine-rich loop region (Fig. 7) This loop also becomes more flexible upon amino acid exchange, which is clearly indicated by the lesser quality of the electron density and the significantly higher B-factors in this region (Fig. 8).

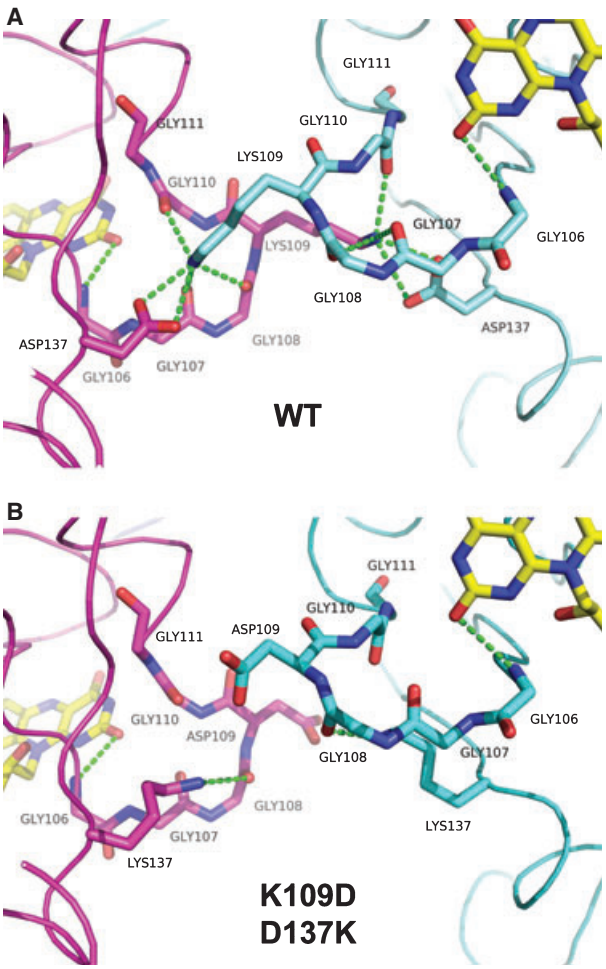

Fig. 5. Close-up view of a portion of the dimer–dimer interface. One subunit is shown in light blue; the other in magenta. The FMN cofactor is shown in yellow; hydrogen bonding interactions are indicated using dashed green lines. (A) In wild-type YhdA, a salt bridge between Lys109 and Asp137 is formed across this interface. (B) In the K109D/D137K variant, the number of interactions is greatly reduced and the salt bridge can no longer be formed. The figure was prepared using the software PYMOL (http://www.pymol.org/).

Discussion

Quinone reductases are present in many different organisms in the eubacterial, fungal, plant and animal kingdom. YhdA, previously described as an azoreductase [8], clearly possesses quinone reductase activity. Considering the similarity of YhdA both in sequence and structure with confirmed quinone reductases such as mammalian NQO1 and yeast Lot6p, this finding is not unexpected. On the other hand, YhdA differs with regard to its quaternary structure. Although quinone reductases of eukaryotic origin form dimers, YhdA assembles into a tetramer, made up by a dimer of dimers (Scheme 1 and Fig. 4). The reasons for adopting higher quaternary protein structures are still elusive and appear to be case-dependent. Comparisons of the quaternary structure of proteins from thermophilic organisms with their mesophilic counterparts have indicated that higher oligomeric structures provide increased thermal stability required for adaptation to elevated temperatures [13,21,22]. Although *B. subtilis* is not a thermophilic organism, YhdA possesses a surprisingly high thermal stability, with an apparent melting temperature of T_m = 86.5 °C. By contrast to YhdA, its ortholog from *Saccharomyces cerevisiae* has a much lower apparent melting temperature (T_m = 60.2 °C), as could be expected as a result of its lower quaternary structure. Inspection of the tetrameric structure of YhdA revealed that the main contacts between the two dimers are set up by four reciprocal salt bridges between the side chains of K109 and D137 (Scheme 1). Therefore, we hypothesized that these interactions are responsible for tetramer stabilization and this in turn will lead to increased thermostability. Based on this hypothesis, we generated two variants with either K109 or D137 replaced by leucine and a third variant with both residues exchanged to leucine. In a fourth variant, we swapped the interacting residues in an attempt to restore the salt bridge and thus redesign an intact dimer–dimer interaction. The role of the salt bridges for tetramer assembly was confirmed by our experimental results because the two single replacement variants were exclusively found as dimers both in solution and in the crystal. The two double variants predominantly exist as dimers in solution, although both showed some tendency to form tetramers in solution (Fig. 3 and Table 2). In the crystal, both of them were clearly present as tetramers showing packing similar to the wild-type protein (Fig. 6). Interestingly, inverting the position of the interaction partners in the K109D/D137K protein variant does not rebuild the salt bridge, as is clearly seen in the crystal structure (Fig. 5B). Instead, K137 forms a hydrogen bond to the backbone C=O of G108 and not to the carboxyl group of D109.

However, none of the protein variants exhibited decreased thermostability (Table 2), clearly contradicting our initial hypothesis that tetramer assembly is responsible for higher thermostability. Obviously, thermostability in this case is not a function of quaternary structure but an intrinsic property of YhdA protomers and/or the dimer.

Surprisingly, quinone reductase activity was severely compromised in all variants because of a lack of reduction of the FMN cofactor by NADPH. This was clearly unexpected because all variants appear to have

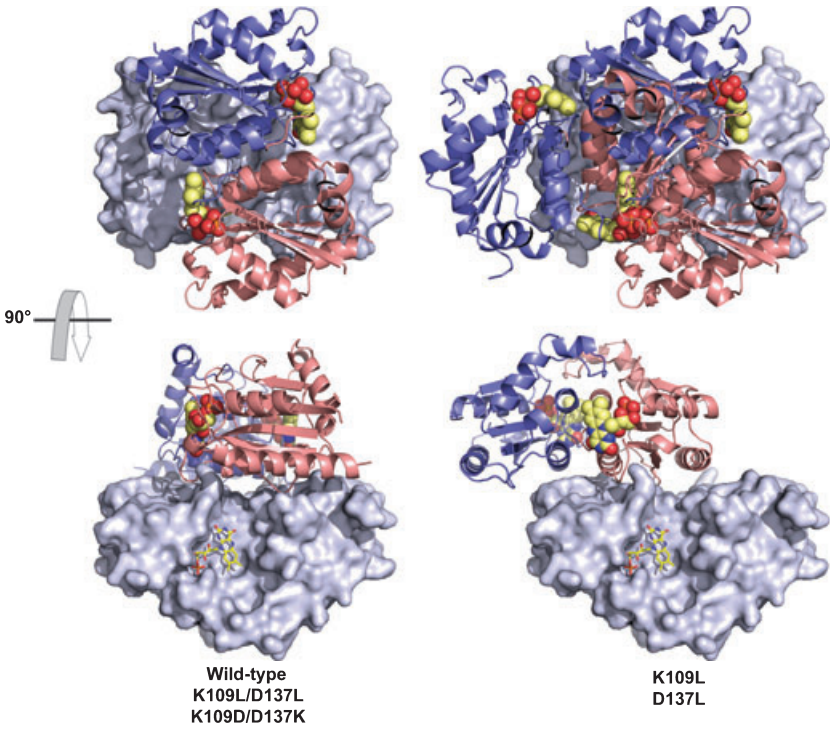

Fig. 6. Schematic representation of the observed oligomeric states and dimer–dimer interactions in different YhdA variants. In each case, one two-fold symmetric dimer subunit is shown in its surface representation, whereas the other is shown in a cartoon representation. Two views are presented, which are rotated by 90° around the *x*-axis. Wild-type YhdA, as well as the double replacement variants, form stable tetramers with the two dimers rotated by approximately 60° relative to each other (left). In the single replacement variants (right), the two dimers are oriented parallel to each other. The latter interaction is only present in the crystal. The figure was prepared using the software PYMOL (http://www.pymol.org/).

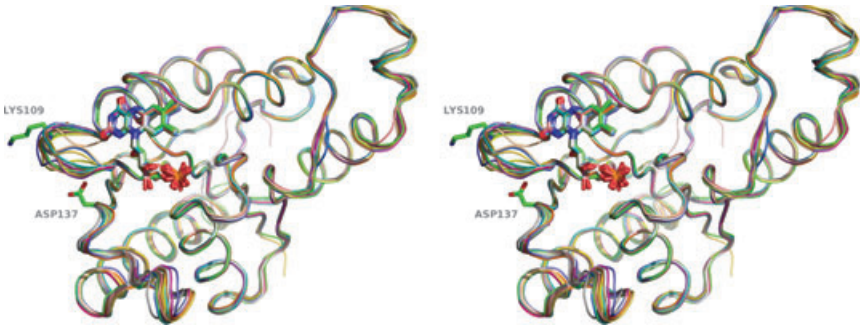

Fig. 7. Stereo representation of the superposition of all YhdA protomers found in the crystal structures of the wild-type (PDB entry: 1nni) and the different variants. In total, 21 structures are shown in different colours. The two sites of amino acid exchanges are indicated. The protomer structures are very similar to each other (for details, see text) and differ only in some loop regions, especially around residues 109 and 137. The figure was prepared using the software PYMOL (http://www.pymol.org/).

similar active sites as judged by their UV/visible absorbance spectrum. Moreover, initially, the determined structures of the variants showed no conspicuous differences that would have predicted altered enzymatic properties. Closer inspection, however, revealed that a glycine-rich loop in the vicinity of the isoalloxazine ring system with Gly106 directly interacting with C(2=O) of the pyrimidine moiety shows substantially altered mobility (Fig. 8). In wild-type YhdA, this loop is stabilized by K109 of a neighbouring subunit (Scheme 1 and Fig. 5); in the variants, this interaction is lost either as a result of replacement of the lysine residue or, in the case of the D137L variant, by abrogated tetramer formation. It appears that the higher mobility of the glycine-rich loop is incompatible with binding of NADPH and/or delivery of a hydride to the flavin cofacor and hence K109 plays a dual role by supporting tetramer assembly through its interaction with D137 and stabilization of the glycine-rich loop necessary to enable flavin reduction by NADPH. Unfortunately, attempts to obtain a crystal structure with NADPH or $NADP^+$ bound to the active site have so far proved unsuccessful (for a model, see Fig. S1).

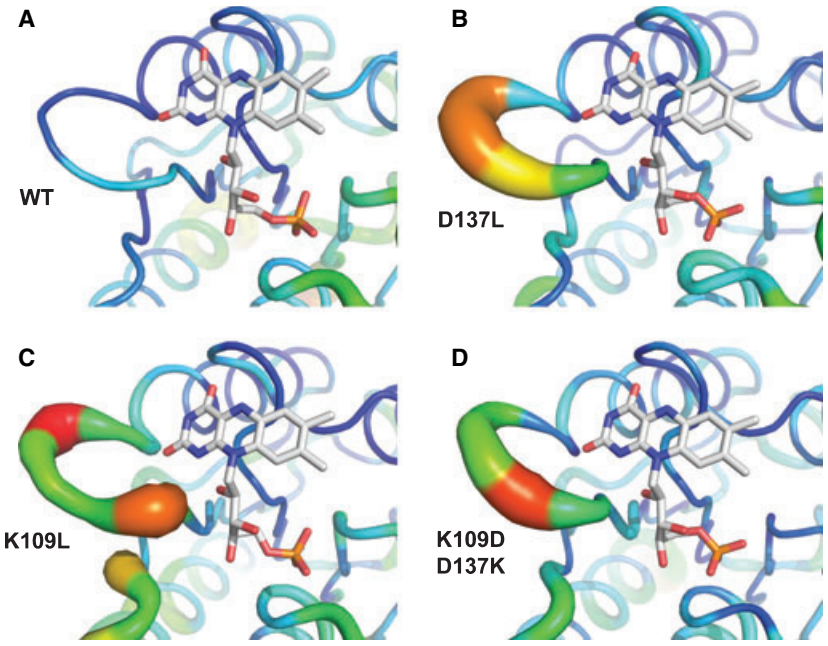

Fig. 8. 'B-factor putty' representation of structures of different YhdA variants (A, wild-type; B, D137L; C, K109L; D, K109D/D137K) focusing in the glycine-rich loop around residue 109. Orange to red colours and a wider tube indicate regions with higher B-factors, whereas shades of blue and a narrower tube indicate regions with lower B-factors. The FMN cofactor is shown as a stick representation. The figure was prepared using the software PYMOL (http://www.pymol.org/).

The findings obtained in the present study suggest that tetramer assembly of YhdA is not responsible for the unusual thermostability; however, the quaternary structure appears to be required for catalytic activity. Although wild-type enzyme clearly exists as a tetramer in solution, it is conceivable that extreme environmental conditions (e.g. high temperature) may cause dissociation of the tetramer into dimers and hence result in the deactivation of quinone reductase activity. Because YhdA dimers exhibit the same thermal stability as tetramers, this mode of regulation is reversible (i.e. tetramers can reform once conditions favouring tetramer assembly are restored). At this point, it is not clear whether regulation of quinone reductase activity through reversible dimer–tetramer equilibrium is relevant for the bacterium and to which end it serves in adaptation to environmental challenges.

Experimental procedures

Reagents

The Ni-NTA was obtained from Qiagen (Hilden, Germany). All chemicals were of the highest grade commercially available and obtained from Sigma-Aldrich (St Louis, MO, USA), Fluka (Buchs, Switzerland), Merck (Darmstadt, Germany), or Carl Roth GmbH (Karlsruhe, Germany).

Cloning, recombinant expression and purification

The cloning of *yhdA* from *B. subtilis* into the pET21a vector, the recombinant expression of YhdA using the host expression strain *Escherichia coli* BL21 (DE3) and the protein purification procedure have been described previously [8]. The Sephadex Desalting Column PD-10 from GE Healthcare (Amersham, UK) was used for buffer exchange.

Site-directed mutagenesis

Site-directed mutagenesis was carried out as specified in the QuikChange® XL Site-Directed Mutagenesis Kit from Stratagene (Cedar Creek, TX, USA). The pETyhdA plasmid described previously [8] served as a template, performing the PCR-based mutagenesis. To obtain the two single muteins YhdA K109L and YhdA D137L, as well as the two double muteins YhdA K109L/D137L and YhdA K109D/D137K, the following primers and their complementary counterparts were used: K109L: 5′-GGG CGG CGG ACTT GGC GGC ATC AAT G-3′ (sense), D137L: 5′-GCA GCT GGT GCT TCT TCC GGT GCA TAT TG-3′ (sense), K109D: 5′-GGG CGG CGG AGA TGG CGG CAT CAA TG-3′ (sense), D137K: 5′-GCA GCT GGT GCT TAA ACC GGT GCA TAT TG-3′ (sense) (where the underlined nucleotides represent the mutated codon). After the mutagenesis protocol, the sequences of the transformation constructs were verified by sequencing analysis. The generation of the double mutations was achieved using pETyhdA(K109L) and pETyhdA(D137L), respectively, as templates and the relating primer pairs for the PCR. The mutated plasmids were purified according to the Plasmid DNA Purification Kit from Macherey-Nagel (Düren, Germany) and transformed into the host expression strain *E. coli* BL21 (DE3). Recombinant expression of the protein variants and the purification procedure by Ni-NTA chromatography were performed as described for the wild-type enzyme [8].

Molecular mass determination

For the native molecular mass determination of the variants, molecular sieve chromatography was used [8]. The results obtained from the molecular sieve chromatography were verified by native PAGE, in accordance with the standard procedures for SDS-PAGE, using 12.5% separating gels and 5% stacking gels. The gels and the running buffer, respectively lacked SDS or dithiothreitol to maintain the native state of proteins. Native PAGE was performed for 4 h at 90 V and 4 °C. In addition, DLS of wild-type YhdA and the four protein variants was carried out with a DynaPro™ (Wyatt Technology, Santa Barbara, CA, USA).

Spectrophotometric methods

To determine the extinction coefficient of enzyme-bound FMN, 0.2% SDS was used to release the cofactor. UV/visible absorbance spectra were recorded before and after denaturation of the enzyme with a photometer (model specord 205) from Analytik Jena AS (Jena, Germany). All measurements were performed in 100 mM Tris/HCl (pH 7.5) using 1 cm quartz cuvettes, unless stated otherwise.

Steady-state kinetics

To determine the reaction mechanism, steady-state turnover of wild-type YhdA was measured by monitoring the oxidation of NADPH spectrophotometrically in the presence of 2-hydroxy-*p*-naphthoquinone. Steady-state turnover of the protein variants was determined by monitoring the oxidation of NADPH in the presence of molecular dioxygen as substrate. Initial velocities were measured by monitoring the decrease in A_{340}. All reactions were carried out in 100 mM Tris-HCl (pH 7.5) at 37 °C. The reaction mixture contained 4 μM enzyme, 10 μM FMN, and NADPH in the concentration range 25–275 μM. The enzyme activity was calculated by using a molar absorption coefficient of 6220 $M^{-1}\cdot cm^{-1}$ for NADPH.

Determination of the stereospecificity of YhdA

YhdA was exchanged into appropriate buffer (30 mM Tris-HCl, pH 8.0, in D_2O) using Econo-Pac 10DG desalting columns (Bio-Rad, Hercules, CA, USA). A solution (1 mL) containing the buffer mentioned above, 10 μM YhdA, and 3 mg of either [4*R*-^{2}H]-NADPH or [4*S*-^{2}H]-NADPH was left to react for 2 h at 37 °C. Enzyme was removed using size-exclusion chromatography, the remaining solution was lyophilized, and the product analyzed by ^{1}H-NMR [23]. All listed signals are given relative to tetramethylsilane as an internal standard.

Stopped-flow kinetics

Stopped-flow measurements were carried out with a Hi-Tech (SF-61DX2) stopped-flow device (TgK Scientific Limited, Bradford-on-Avon, UK) positioned in a glove box from Belle Technology (Weymouth, UK) at 25 °C. Two reactant solutions were joined in single mixing mode, using a 0.5 mL stopping syringe. FMN oxidation and reduction were measured respectively, by monitoring changes in A_{453} with a KinetaScanT diode array detector (MG-6560) (TgK Scientific Limited). Initial rates were calculated by fitting the curves with SPECFIT 32 (Spectrum Software Associates, Chapel Hill, NC, USA) using a function of two exponentials.

To perform the reductive half reaction, 40 μM enzyme and NADPH at a concentration in the range 0.5–8.0 mM in 100 mM Tris-HCl (pH 7.5) were mixed by the stopped-flow device. The decrease in A_{453} was monitored spectrophotometrically.

To determine rate constants for the oxidative half reaction, 40 μM enzyme in 100 mM Tris-HCl (pH 8.4) was first reduced chemically by titration of 14 mM sodium dithionite. After mixing with 2-hydroxy-*p*-naphthoquinone at concentrations in the range 25–500 μM, the reoxidation of the FMN cofactor was monitored by measuring A_{453}. For preparation of the quinone solution, a 10 mM stock solution of 2-hydroxy-*p*-naphthoquinone in ethanol was diluted with 100 mM Tris-HCl (pH 8.4) to the final concentrations. All samples were prepared by flushing with nitrogen followed by incubation in the glove box environment.

Thermal unfolding experiments

Thermal unfolding of the muteins was monitored in 0.1 cm cuvettes using a Jasco J-500 spectropolarimeter (Jasco Inc., Easton, MD, USA) at 225 nm. The cuvette was placed in a thermostated cell holder. The temperature was raised continuously from 5 to 95 °C at a heating rate of 1 $°C\cdot min^{-1}$. The enzyme concentration was 50 μM, in 100 mM Tris-HCl (pH 7.5). DSC was performed with a VP-DSC, MicroCal calorimeter (MicroCal Inc., Northampton, MA, USA). After scanning a buffer–buffer baseline of 100 mM Tris-HCl (pH 7.5), 600 μL samples containing 1–3 $mg\cdot mL^{-1}$ protein were scanned at a heating rate of 1 $°C\cdot min^{-1}$ at a temperature in the range 5–110 °C.

X-ray crystal structures

The YhdA variants were crystallized at room temperature using the batch crystallization method with drops of 1 μL of protein solution (c = 10–18 $mg\cdot mL^{-1}$) plus 1 μL of reservoir solution. Diffraction quality crystals were obtained under the conditions: 0.1 M Hepes (pH 7.5), 0.2 M $(NH_4)_2SO_4$, 25% w/v PEG 3350 (K109L variant); 0.1 M Bis-Tris (pH 6.5), 20% w/v PEG MME 5000 (D137L

variant); 0.1 M Tris-HCl (pH 8.5), 2.0 M $(NH_4)_2SO_4$ (K109D/D137K variant); 0.1 M Hepes (pH 7.0), 0.2 M $(NH_4)_2SO_4$, 0.5% w/v PEG 8000 (K109L/D137L variant). For cryoprotection, the crystals were transferred to corresponding solutions containing 25% glycerol before flash-cooling in liquid nitrogen.

Diffraction datasets were collected at beamlines X13 (λ = 0.8148 Å) and X11 (λ = 0.8010 Å) at the DESY/EMBL (Hamburg, Germany). In all cases, data reduction involved the HKL software package [24], as well as software from the CCP4 suite [25].

The structures were solved by molecular replacement with the software PHASER [26] using the structure of wild-type YhdA (PDB entry: 1NNI) as a search model and were further refined using the software PHENIX [27]. Model building and fitting steps involved the graphics software COOT [28] using σ_A-weighted $2F_o$–F_c and F_o–F_c electron density maps [29]. R_{free}-values [30] were computed from 5% randomly chosen reflections that were not used throughout the refinement. In the higher resolution structures, water molecules were placed automatically into difference electron density maps and were retained or rejected based on geometric criteria, as well as on their refined B-factors. NCS restraints were applied during all refinement steps. Details of the data collection, processing and structure refinement are summarized in Table 4. Molprobity Ramachandran plots [31] showed no outliers in the higher resolution structures (D137L and K109D/D137K) and 0.6% outliers in the lower resolution structure (K109L). The coordinates and structure factors have been deposited with the PDB under accession numbers 3GFQ (K109L), 3GFR (D137L) and 3GFS (K109D/D137K).

Acknowledgements

We appreciate the support of staff scientists at the synchrotron beamlines at DESY/EMBL (Hamburg, Germany) during the diffraction data collection. Support provided by the Austrian Science Fund (FWF) through *Doktoratskolleg* 'Molecular Enzymology' (W901-B05) to K.G. and P.M. is gratefully acknowledged.

References

1 Bin Y, Jiti Z, Jing W, Cuihong D, Hongman H, Zhiyong S & Yongming B (2004) Expression and characteristics of the gene encoding azoreductase from *Rhodobacter sphaeroides* AS1.1737. *FEMS Microbiol Letters* **236**, 129–136.

2 Blümel S, Knackmuss H-J & Stolz A (2002) Molecular cloning and characterization of the gene coding for the aerobic azoreductase from *Xenophilus azovorans* KF46F. *Appl Environ Microbiol* **68**, 3948–3955.

3 Blümel S & Stolz A (2003) Cloning and characterization of the gene coding for the aerobic azoreductase from *Pigmentiphaga kullae* K24. *Appl Microbiol Biotechnol* **62**, 186–190.

4 Chen H, Hopper SL & Cerniglia CE (2005) Biochemical and molecular characterization of an azoreductase from *Staphylococcus aureus*, a tetrameric NADPH-dependent flavoprotein. *Microbiology* **151**, 1433–1441.

5 Chen H, Wang R-F & Cerniglia CE (2004) Molecular cloning, overexpression, purification, and characterization of an aerobic FMN-dependent azoreductase from *Enterococcus faecalis*. *Protein Expr Purif* **34**, 302–310.

6 Nakanishi M, Yatome C, Ishida N & Kitade Y (2001) Putative ACP phosphodiesterase gene (acpD) encodes an azoreductase. *J Biol Chem* **276**, 46394–46399.

7 Suzuki Y, Yoda T, Ruhul A & Sugiura W (2001) Molecular cloning and characterisation of the gene coding for azoreductase from *Bacillus* sp. OY1-2 isolated from soil. *J Biol Chem* **276**, 9059–9065.

8 Deller S, Sollner S, Trenker-El-Toukhy R, Jelesarov I, Gubitz GM & Macheroux P (2006) Characterization of a thermostable NADPH:FMN oxidoreductase from the mesophilic bacterium *Bacillus subtilis*. *Biochemistry* **45**, 7083–7091.

9 Deller S, Macheroux P & Sollner S (2008) Flavin-dependent quinone reductases. *Cell Mol Life Sci* **65**, 141–160.

10 Li R, Bianchet MA, Talalay P & Amzel LM (1995) The three-dimensional structure of NAD(P)H:quinone reductase, a flavoprotein involved in cancer chemoprotection and chemotherapy: mechanism of the two-electron reduction. *Proc Natl Acad Sci USA* **92**, 8846–8850.

11 Liger D, Graille M, Zhou C-Z, Leulliot N, Quevillon-Cheruel S, Blondeau K, Janin J & van Tilbeurgh H (2004) Crystal structure and functional characterization of yeast YLR011wp, an enzyme with NAD(P)H-FMN and ferric iron reductase activities. *J Biol Chem* **279**, 34890–34897.

12 Sollner S, Nebauer R, Ehammer H, Prem A, Deller S, Palfey BA, Daum G & Macheroux P (2007) Lot6p from *Saccharomyces cerevisiae* is a FMN-dependent reductase with a potential role in quinone detoxification. *FEBS J* **274**, 1328–1339.

13 Dams T, Auerbach G, Bader G, Jacob U, Ploom T, Huber R & Jaenicke R (2000) The crystal structure of dihydrofolate reductase from *Thermotoga maritima*: molecular features of thermostability. *J Mol Biol* **297**, 659–672.

14 Murzin AG, Brenner SE, Hubbard T & Chothia C (1995) SCOP: a structural classification of proteins database for the investigation of sequences and structures. *J Mol Biol* **247**, 536–540.

15 Krissinel E & Henrick K (2004) Secondary-structure matching (SSM), a new tool for fast protein structure

alignment in three dimensions. *Acta Crystallogr* **60**, 2256–2268.
16 Agarwal R, Bonanno JB, Burley SK & Swaminathan S (2006) Structure determination of an FMN reductase from *Pseudomonas aeruginosa* PA01 using sulfur anomalous signal. *Acta Crystallogr* **62**, 383–391.
17 Ye J, Yang HC, Rosen BP & Bhattacharjee H (2007) Crystal structure of the flavoprotein ArsH from *Sinorhizobium meliloti*. *FEBS Lett* **581**, 3996–4000.
18 Nissen MS, Youn B, Knowles BD, Ballinger JW, Jun SY, Belchik SM, Xun L & Kang C (2008) Crystal structures of NADH:FMN oxidoreductase (EmoB) at different stages of catalysis. *J Biol Chem* **283**, 28710–28720.
19 Vorontsov II, Minasov G, Brunzelle JS, Shuvalova L, Kiryukhina O, Collart FR & Anderson WF (2007) Crystal structure of an apo form of *Shigella flexneri* ArsH protein with an NADPH-dependent FMN reductase activity. *Protein Sci* **16**, 2483–2490.
20 Krissinel E & Henrick K (2007) Inference of macromolecular assemblies from crystalline state. *J Mol Biol* **372**, 774–797.
21 Thoma R, Hennig M, Sterner R & Kirschner K (2000) Structure and function of mutationally generated monomers of dimeric phosphoribosylanthranilate isomerase from *Thermotoga maritima*. *Structure* **8**, 265–276.
22 Walden H, Bell GS, Russell RJM, Siebers B, Hensel R & Taylor GL (2001) Tiny TIM: a small, tetrameric, hyperthermostable triosephosphate isomerase. *J Mol Biol* **306**, 745–757.
23 Ottolina G, Riva S, Carrea G, Danieli B & Buckmann AF (1989) Enzymatic synthesis of [4R-2H]NAD(P)H and [4S-2H]NAD(P)H and determination of the stereospecificity of 7 alpha- and 12 alpha hydroxysteroid dehydrogenase. *Biochim Biophys Acta* **998**, 173–178.
24 Otwinowski Z & Minor W (1997) Processing of x-ray diffraction data collected in oscillation mode. *Methods Enzymol* **276**, 307–326.
25 CCP4 (1994) The CCP4 suite – programs for protein crystallography. *Acta Crystallogr* **50**, 760–763.
26 McCoy AJ, Grosse-Kunstleve RW, Adams PD, Winn MD, Storoni LC & Read RJ (2007) Phaser crystallographic software. *J Appl Crystallogr* **40**, 658–674.
27 Adams PD, Grosse-Kunstleve RW, Hung LW, Ioerger TR, McCoy AJ, Moriarty NW, Read RJ, Sacchettini JC, Sauter NK & Terwilliger TC (2002) PHENIX: building new software for automated crystallographic structure determination. *Acta Crystallogr* **58**, 1948–1954.
28 Emsley P & Cowtan K (2004) Coot: Model-building tools for molecular graphics. *Acta Crystallogr D Biol Crystallogr* **60**, 2126–2132.
29 Read RJ (1986) Improved Fourier coefficients for maps using phases from partial structures with errors. *Acta Crystallogr* **42**, 140–149.
30 Kleywegt GJ & Brunger AT (1996) Checking your imagination – applications of the free R-value. *Structure* **4**, 897–904.
31 Lovell SC, Davis IW, Arendall WB III, de Bakker PI, Word JM, Prisant MG, Richardson JS & Richardson DC (2003) Structure validation by Calpha geometry: phi,psi and Cbeta deviation. *Proteins* **50**, 437–450.

Supporting information

The following supplementary material is available:
Fig. S1. Structure of the docked YhdA-NADP(H) complex.

This supplementary material can be found in the online article.

Please note: As a service to our authors and readers, this journal provides supporting information supplied by the authors. Such materials are peer-reviewed and may be re-organized for online delivery, but are not copy-edited or typeset. Technical support issues arising from supporting information (other than missing files) should be addressed to the authors.